Selective Synthesis and Luminescence Properties of Self-Assembled $SrMoO_4$ Superstructures via a Facile Sonochemical Route

Chang-Jie Mao,[†,‡] Jun Geng,[†] Xing-Cai Wu,*[,†] and Jun-Jie Zhu*[,†]

Key Lab of Analytical Chemistry for Life Science (MOE), School of Chemistry & Chemical Engineering, Nanjing University, Nanjing 210093, P. R. China, and Department of Chemistry, Anhui University, Hefei 230039, P. R. China

Received: August 5, 2009; Revised Manuscript Received: December 26, 2009

Highly ordered $SrMoO_4$ 3D spherical superstructure assembled with nanosheets was synthesized via a facile and fast sonochemical route without any template. The products were characterized by X-ray diffraction, field emission scanning electron microscopy, transmission electron microscopy, and selected-area electron diffraction. The results showed that the as-synthesized self-assembled $SrMoO_4$ spheres were composed of nanosheets with thickness of about 40−60 nm and width of 1 μm. The pH values and surfactants play an important role in the morphologies of the final sample. The possible mechanism for the formation of self-assembled $SrMoO_4$ spherical superstructure is proposed. The luminescence properties of these $SrMoO_4$ samples with different morphologies have also been investigated.

Introduction

The fabrication of highly ordered self-assembled superstructures of inorganic materials has attracted considerable attention because of their unique properties and potential applications in science and engineering.[1,2] Great effort has been devoted to explore various methods for the control of shape, size, and structure.[3−8] However, most routes need high temperature, catalysts, sophisticated process, or protection gases, which may result in impurity of the final product, high-cost, or inconvenience. Therefore, it is necessary and important to develop a facial approach to synthesize those materials with controlled shape. Recently, sonochemical method has become an ideal medium to synthesize inorganic materials with controlled morphologies.[9,10] The chemical effects of ultrasound are due to acoustic cavitation, which generates localized hot spots having very high temperatures (>5000 K), pressures (>20 MPa), and cooling rates (>10^7 K/s). Such extreme environments provide a unique platform for the growth of novel nanostructures.[11] Using this simple and spontaneous process, some materials with special morphologies and hierarchical architectures have been successfully synthesized.[12,13]

In the past few years, scheelite-type metal molybdates have received great attention because of their wide applications in industry, such as scintillation detectors, optical devices, magnetic materials, catalysts, and so on.[14−17] Strontium molybdate ($SrMoO_4$) is a typical scheelite-type molybdate and has green luminescence at liquid nitrogen temperature.[18] To enhance its physical properties, differently ordered morphology is usually needed. Hence, a variety of efficient techniques have been carried out on the shape-controlled $SrMoO_4$ crystal to improve its properties. To date, different morphologies, such as particles, sheets, dumbbells, and nanowires, have been successfully synthesized.[16,18−33] For instance, Liu and Huang prepared single-crystalline $SrMoO_4$ nanosheets by aqueous solution route.[30] Chen et al. developed a mineralization method for $SrMoO_4$ microcrystallites with delicate morphologies.[32] Zhang's group synthesized $SrMoO_4$ nanowires by hydrothermal method.[33] However, the organization of $SrMoO_4$ nanostructured subunits into highly ordered superstructures still remains a challenge. Recently, self-assembled hierarchical microstructures have attracted much attention due to the interesting morphology, properties, and potential applications. Hierarchical superstructures with excellent properties have been reported, such as platelike $FeWO_4$ microcrystals,[34] $BaMoO_4$ nestlike nanostructures,[35] carbonated apatite flowers,[36] and so on. Here we introduce a facile and fast sonochemical route as a novel technique to first prepare highly ordered $SrMoO_4$ superstructures. This facile technique offers a general methodology to prepare organized shapes of metal molybdates. It was found that the experimental parameters have great influence on the morphologies of products. The formation mechanism of self-assembled $SrMoO_4$ spheres was proposed in terms of the experimental results. The luminescence properties of $SrMoO_4$ samples with different morphologies have been investigated.

Experimental Section

Synthesis of the Samples. All the reagents were of analytical purity and used without further purification. In a typical synthesis, $Sr(NO_3)_2$ (1 mmol) and Na_2MoO_4 (1 mmol) were added to 40 mL of distilled water under vigorous stirring, respectively, and then the pH value was adjusted to a specific value with HCl solution. The final concentration was 12.5 mmol/L $Sr(NO_3)_2$ and 12.5 mmol/L Na_2MoO_4, and the total volume of the solution was 80 mL. After the above resulting solutions were mixed rapidly, the solution was exposed to high-intensity ultrasound irradiation under ambient air. Ultrasound irradiation was accomplished with a high-intensity ultrasonic probe (Xinzhi. Co., China, JY92-2D, 10 mm diameter; Ti-horn, 20 kHz, 100 W/cm^2) immersed directly in the reaction solution for 30 min. Finally, a white precipitate was centrifuged, washed with distilled water and ethanol, and dried in air.

Characterization. Powder X-ray diffraction (XRD) was performed on a Philip X'pert X-ray diffractometer with Cu Kα

* Authors to whom correspondence should be addressed. E-mail: jjzhu@nju.edu.cn (J.-J.Z); wuxingca@nju.edu.cn (X.-C.W). Tel. and Fax: +86-25-83594976.
† Nanjing University.
‡ Anhui University.

10.1021/jp907525p
Published on Web 01/19/2010

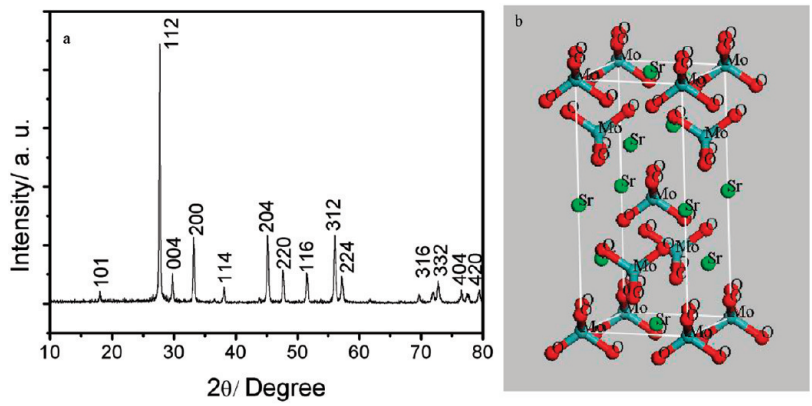

Figure 1. (a) XRD pattern and (b) crystal structure for the obtained $SrMoO_4$ sample.

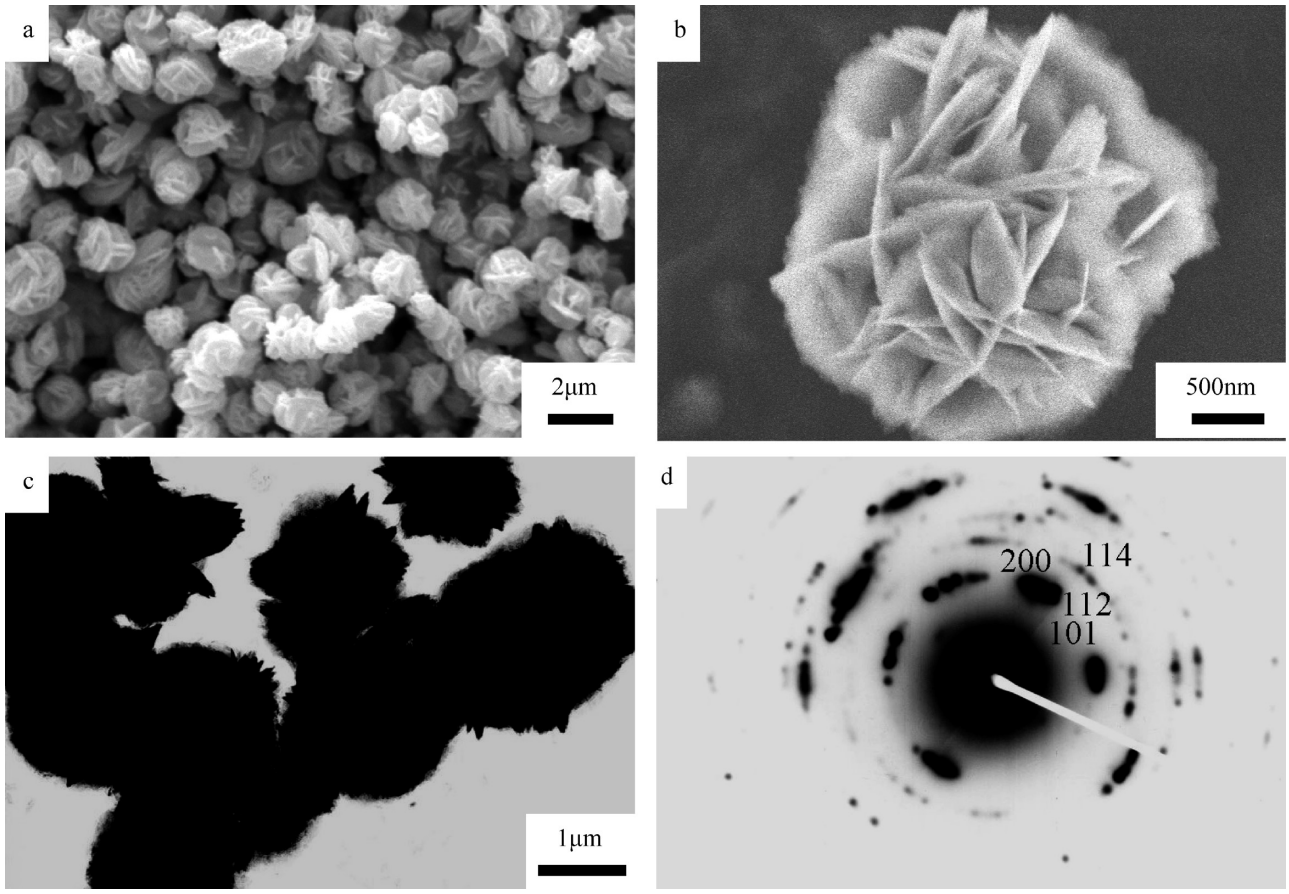

Figure 2. Morphologies of the obtained $SrMoO_4$ samples: (a) a typical SEM image, (b) a higher-magnification SEM image, (c) a typical TEM image, and (d) the SAED pattern.

radiation ($\lambda = 1.5418$ Å). Transmission electron microscopy (TEM) and selected-area electron diffraction (SAED) were measured on a JEOL JEM-200CX, using an accelerating voltage of 120 kV. Scanning electron microscopy (SEM) was taken by a LEO-1530 VP. Fourier transforms infrared (FT-IR) spectroscopy was recorded by a Nicolet 6700. Photoluminescence (PL) spectra were measured on a Shimadzu RF-5301PC fluorescence spectrometer. All spectra were collected at room temperature.

Results and Discussion

Structures and Characterization. Highly ordered $SrMoO_4$ 3D spherical superstructure can be synthesized via a facile sonochemical method. The crystalline phase of the product was studied by XRD. The XRD of the obtained product is shown in Figure 1. It is found that as-synthesized $SrMoO_4$ sample showed good crystallinity. All diffraction peaks can be indexed to the tetragonal system with the lattice constants $a = 5.394$ Å and $c = 12.02$ Å, which are in good agreement with the JCPDS card no. 08-0482. No peaks of any other phases are detected, indicating the high purity of the product. The crystal structure of $SrMoO_4$ is shown in Figure 1b. It is found that the molybdenum atoms coordinated with four oxygen atoms and the strontium atoms coordinated with eight oxygen atoms to form the unit cell of $SrMoO_4$.[32]

The morphology of the obtained $SrMoO_4$ sample was examined by SEM and TEM. As shown in Figure 2a, it is clearly demonstrated that the product consisted of a large amount of spherical structures. The mean diameters of these spheres are

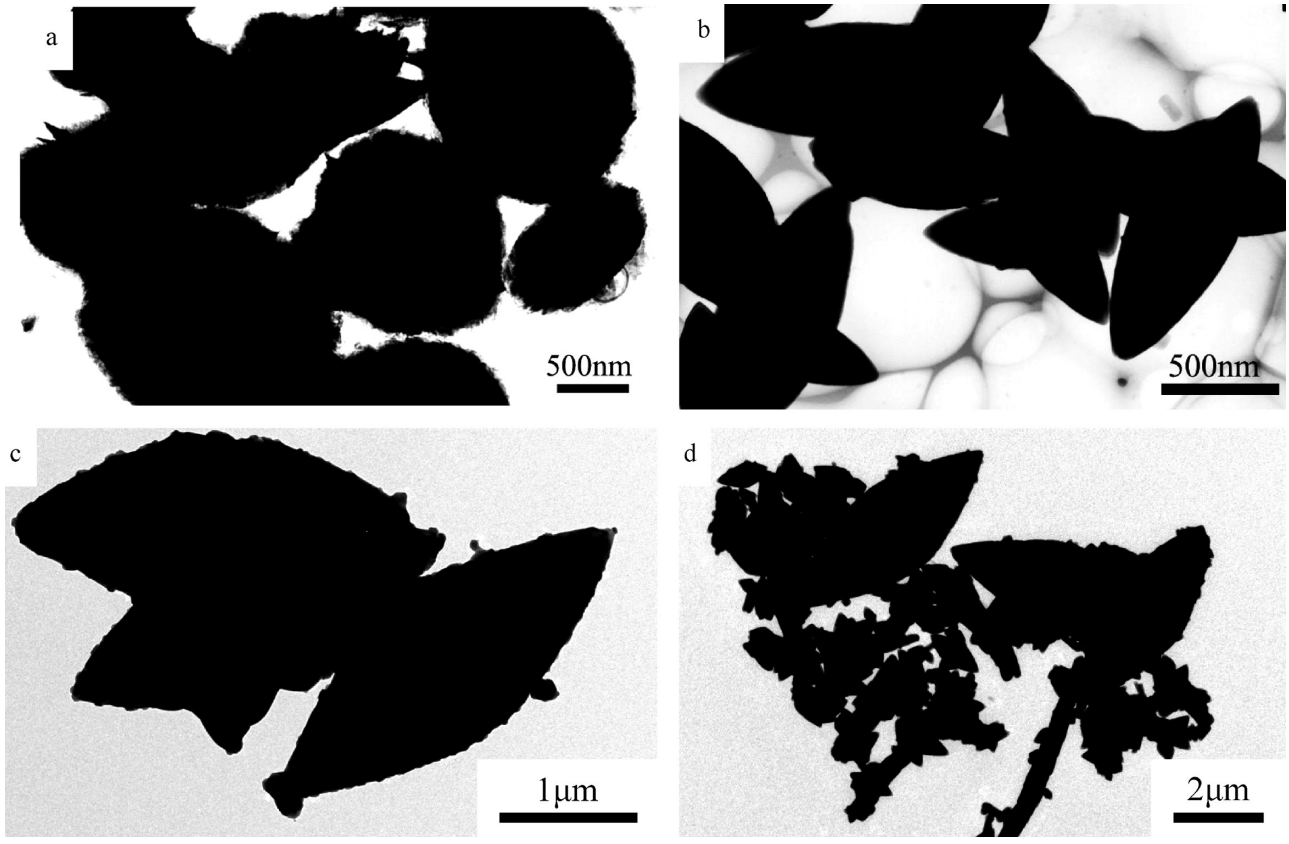

Figure 3. TEM images of $SrMoO_4$ sample prepared at pH of (a) 5.0, (b) 7.0, (c) 9.0, and (d) 11.0.

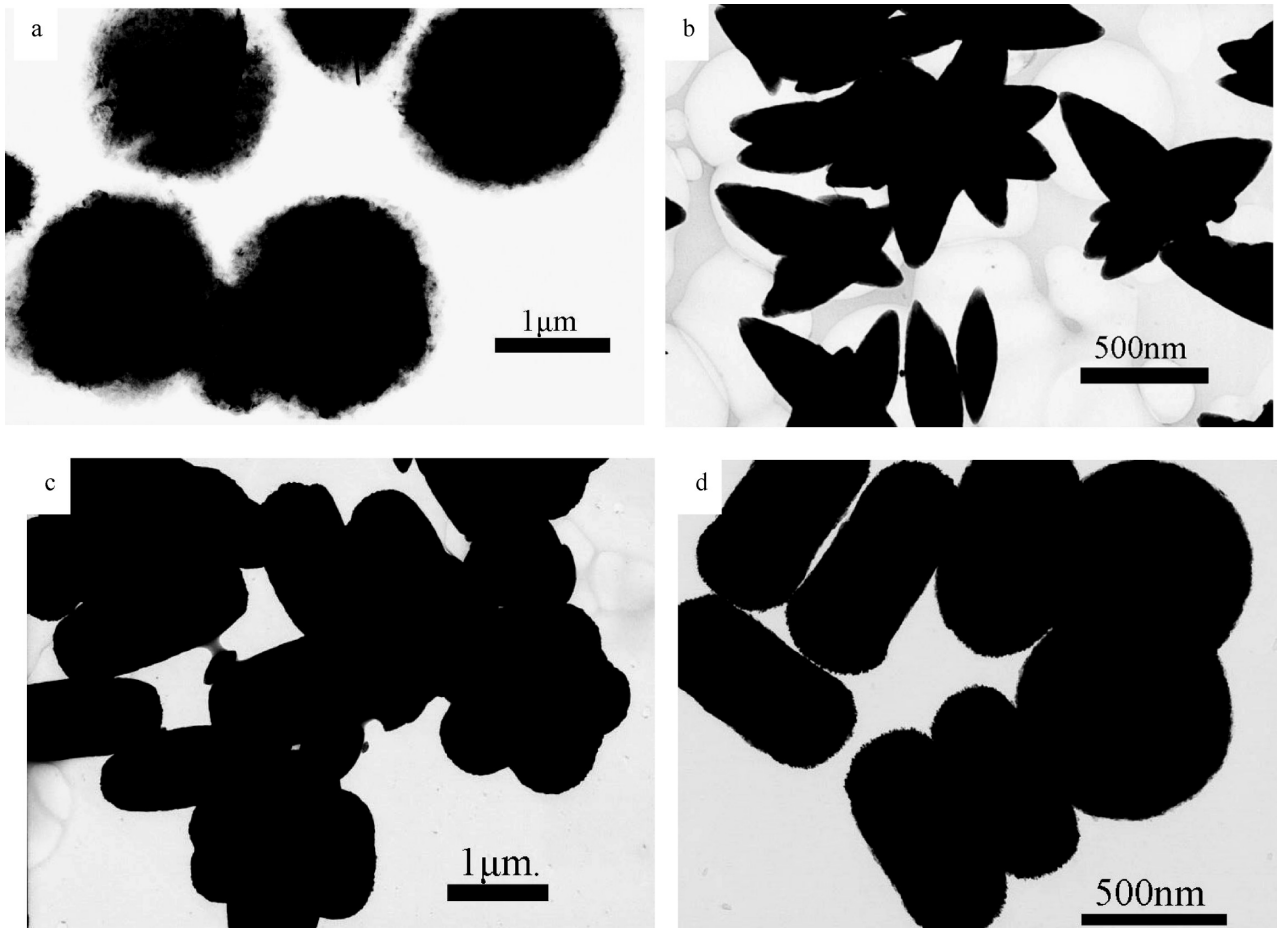

Figure 4. TEM images of $SrMoO_4$ synthesized with different surfactants: (a) 0.5 g of PEG-200 at pH 5, (b) 0.5 g of PEG-200 at pH 7, (c) 0.5 g of gelatin at pH 7, and (d) 0.5 g of gelatin at pH 5.

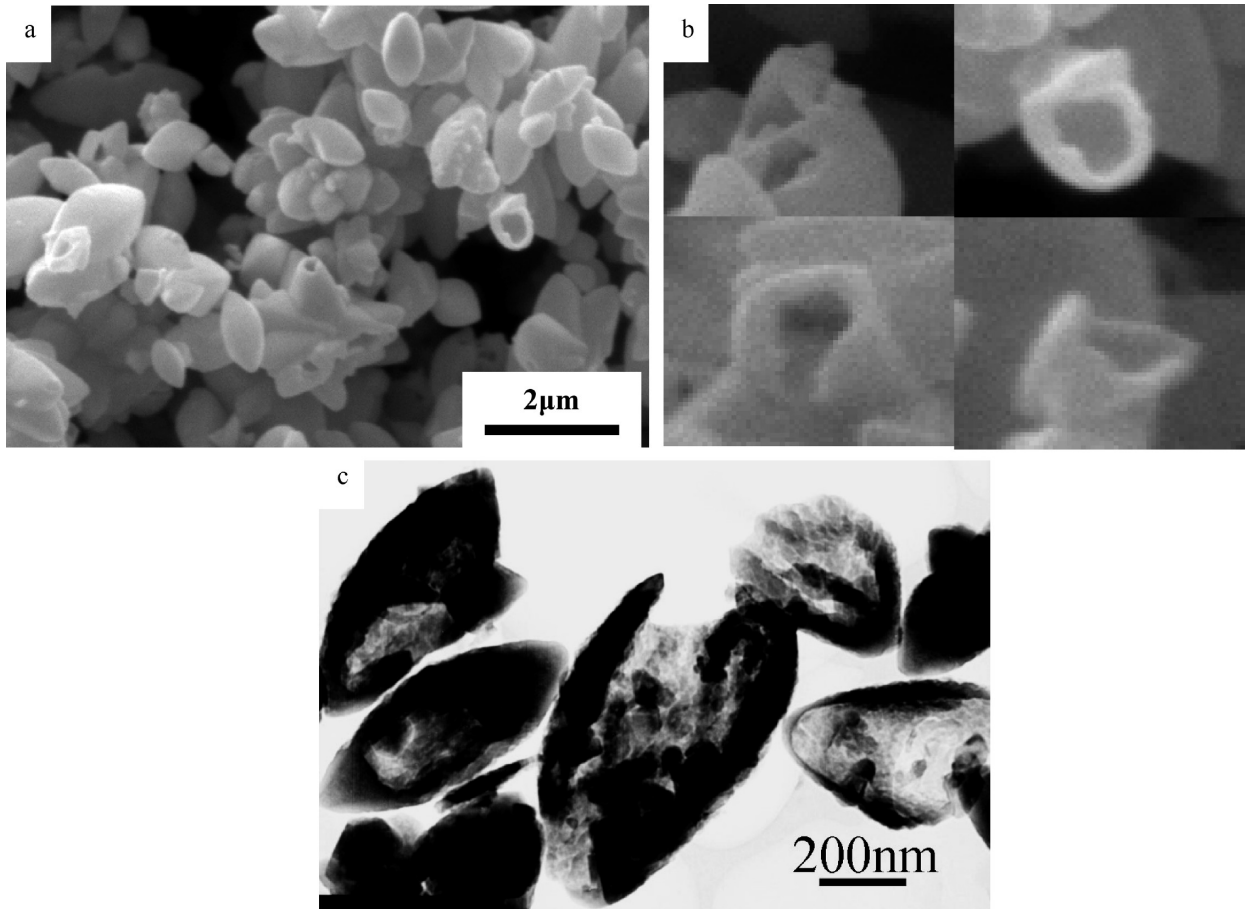

Figure 5. (a) Typical SEM image of the obtained $SrMoO_4$ with 0.5 g of P123. (b) SEM images of several broken hollow spindles viewed from different angles. (c) Typical TEM image of the final product.

about 1 μm. A higher-magnification SEM image (Figure 2b) reveals that an individual sphere is composed of tens of similar nanosheets with thickness of 40−60 nm and width of 0.5−1 μm. These nanosheets are connected with each other to form sphere with random orientation. The morphology and microstructure of the as-synthesized $SrMoO_4$ sample was further studied by TEM (Figure 2c). In agreement with the SEM results, we can distinctly observe that many minute projecting edges attach on the surface of the spheres. This result further confirmed that the individual $SrMoO_4$ sphere is composed of nanosheets. The SAED recorded on an individual $SrMoO_4$ sphere reveals that the final sample is polycrystalline.

Effect of pH Value. pH value is one of the most important factors influencing morphology of the final product. To investigate the influence of pH value on the morphology, the $SrMoO_4$ was prepared at different pH values under the present experimental conditions. In the pH value under 4, no precipitate was observed. When the pH value was increased to 5, the morphology of the products was self-assembled spherical structure. It was found that the sphere is composed of several tens of similar nanosheets as shown in Figure 3a. When the pH value was 7, the morphology of the sample consisted of spindle structure with a mean diameter of 300 nm at the center and lengths of about 2 μm (Figure 3b). When the pH was further increased to 9, some nanoparticles were observed on the surfaces of the spindles structure (Figure 3c). After the pH was increased to 11, the morphology was a mixture of nanoparticles, spindles, and nanorods (Figure 3d), and the product was mixture of $SrMoO_4$ and $Sr(OH)_4$. This is due to the fact that the higher concentration of Sr^{4+} has a more similar combining ability with $[OH]^-$ than $[MoO_4]^-$ in the higher alkali solution.

Effect of Surfactants. Surfactants have special structures and fascinating template functionalities. Many studies have indicated that surfactant-assistant synthesis has been a popular method to achieve morphological control. In our case, it is found that only some kinds of surfactants can influence the morphology of the final sample. When 0.5 g of PVP (poly(vinylpyrrolidone)), PEG (poly(ethylene glycol))-200, PEG-2000, PEG-20000, and SDS (sodium dodecyl sulfate) were added into the reaction system, respectively, the morphologies of all samples were keep unchangeable. When the experiment was carried out under the same conditions via employing above different kinds of surfactants at pH 5, their morphologies were spherical structures with rough surface, and the average diameter was 1 μm (Figure 4a). While the pH was 7, the morphology was spindle (Figure 4b). However, when 0.5 g of gelatin was used, the morphology was changed into rods, and these rods aggregated by each other (Figure 4c). The average length of these rods was about 2 μm, and the diameter was 500 nm. With further increase of the concentration of gelatin, the morphology and size of the final product hardly changed. Further research indicated that pH value had also a significant effect on morphology in this case. When pH changed to 5, mixture of spheres and rods was found, and the surface of their spherical structure changed into smooth (Figure 4d). Gelatin is an amphoteric polyelectrolyte consisting of amino acid groups. It has good adsorption properties due to the fact that the gelatin chains can interact with each other through hydrogen bonding.[37] Although the exact roles of gelatin on the morphological control are still not completely understood, gelatin might play a role as follows. Before the reaction begins, Sr^{2+} and MoO_4^{2-} ions have been protected by gelatin because of the existence of hydrogen bonding between ions and the

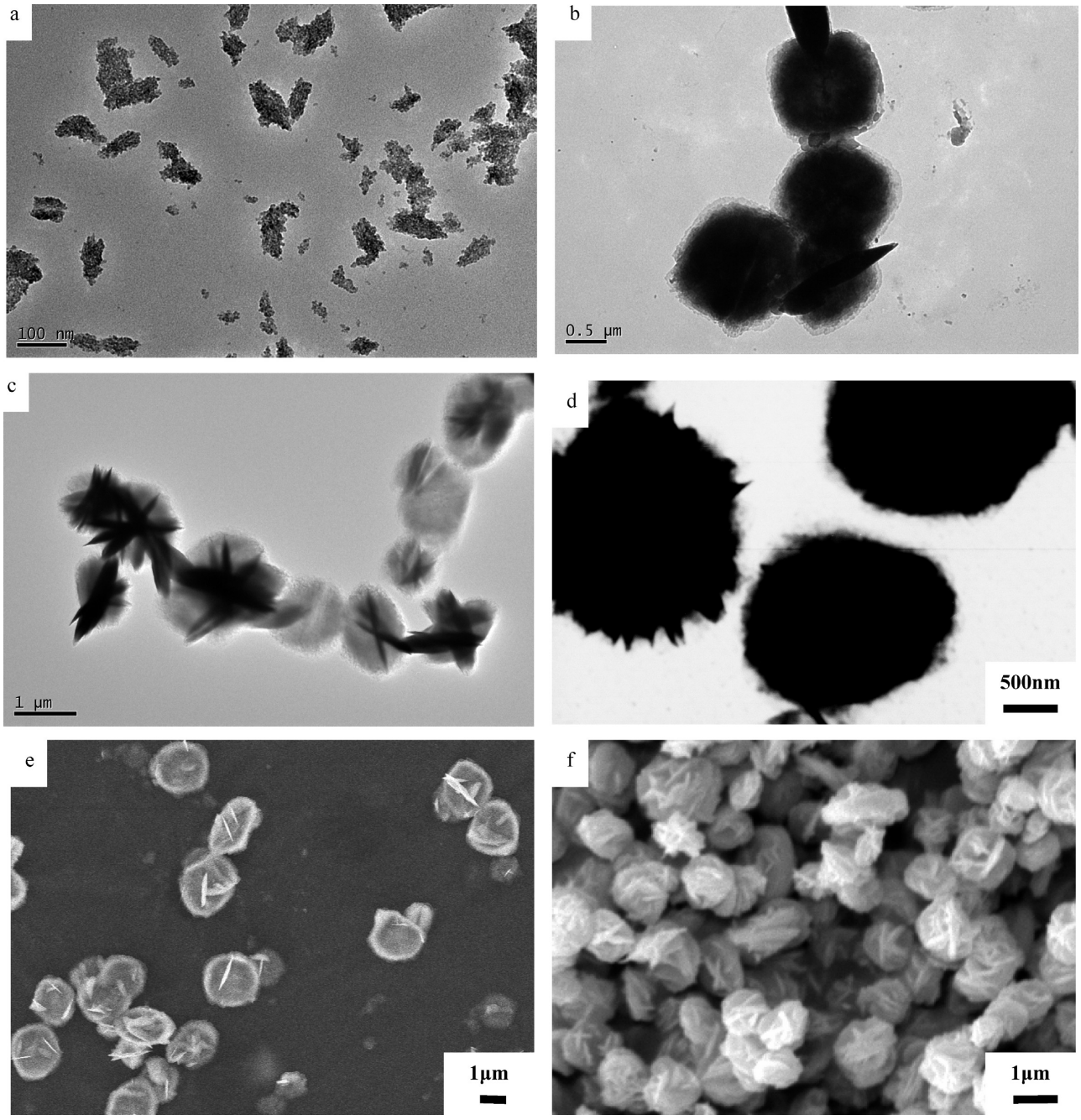

Figure 6. TEM images of the final products obtained at different reaction times of (a) 2, (b) 5, (c) 20, and (d) 30 min. SEM images at the different times of (e) 20 and (f) 30 min, respectively.

gelatin chains. When the reaction system was irradiated with ultrasound, they might attack each other and form initial $SrMoO_4$ nanocrystals. These freshly formed nanocrystals were unstable and could selectively adsorb gelatins due to the high surface activity. The gelatin adsorbed onto some surfaces of $SrMoO_4$ nanocrystals could restrain the growth rates of these surfaces and lead to highly anisotropic growth. This process is the preferential adsorption mechanism.[38]

When 0.5 g of Pluronic amphiphilic triblock copolymer P123 ($EO_{20}PO_{70}EO_{20}$, $M_{Av} = 5800$) was added into the reaction system, the majority of the final sample had a uniform spindle shape with diameter of 500 nm at the center and length of about 2 μm (Figure 5a). It is found that a few partly broken hollow spindles can be clearly observed. Figure 5b shows several broken hollow spindles viewed from different angles. The morphology of the as-synthesized $SrMoO_4$ was further studied by TEM. It is clearly found that a strong contrast difference exists between the edges (dark) and centers (bright) and hollow interior with wall thickness of about 50 nm in Figure 5c. P123 possesses a dehydrated PPO segment and two hydrated PEO blocks. When the polymer concentration exceeds the critical micelle concentration (cmc), the P123 core−shell micelles are formed and are able to bind with metal ions.[39] Pb^{2+} ions easily form Pb−(PEO−PPO−PEO) units on the micellar surfaces, which provide nucleation domains to form nascent $SrMoO_4$ nanoparticles. In the later growth stage, the freshly $SrMoO_4$ nanoparticles further form $SrMoO_4$ layer on the surface of the micellar aggregates. The micellar templates can be eliminated by the subsequent washing process. This process is the template mechanism and similar to other hollow structures.[40,41]

Possible Growth Mechanism. In order to understand the morphological evolution, time-dependent experiments were

SCHEME 1: Schematic Illustration of the Formation of the Obtained $SrMoO_4$ with Different Morphologies under Ultrasound Treatment

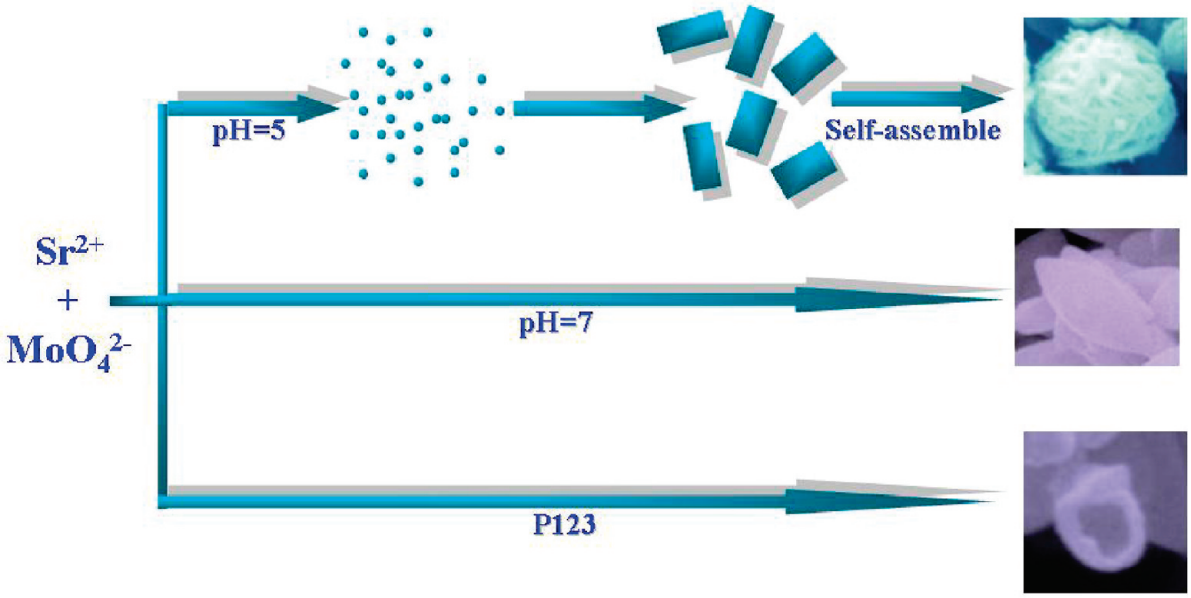

performed. In the case of the self-assembled $SrMoO_4$ spherical superstructure, the samples were characterized by TEM at different reaction times. Figure 6 showed the images taken from the reaction mixture after the solution was exposed to high-intensity ultrasound irradiation for 2, 5, 20, and 30 min. In Figure 6a, TEM images of the early growth stage of $SrMoO_4$ showed that $SrMoO_4$ nanoparticles were obtained after ultrasound irradiation for 2 min. With the ultrasound proceeding, the nanosheets began to appear (Figure 6b), but small particles still existed. When the reaction time reached 20 min, these nanosheets began to assemble into sphere clusters, and the typical 3D sphere structure was formed (Figure 6c). At the reaction time of 30 min, the reaction reached a stable state. The growth of the $SrMoO_4$ sample was also confirmed by SEM (Figure 6e and 6f). To make a comparison, we have also carried out the reaction with vigorous electromagnetic stirring instead of ultrasound irradiation. The final products are mainly amorphous particles. The experiments proved that high-intensity ultrasonic irradiation played an important role in the formation of self-assembled $SrMoO_4$ superstructure.

On the basis of the experimental results, a possible formation mechanism was proposed. We believe that the sonochemical formation of self-assembled $SrMoO_4$ sphere superstructures underwent three steps: (1) ultrasound-induced formation of $SrMoO_4$ nanoparticles, (2) these primary nanoparticles accompanying oriented attachment to form nanosheets, and (3) these nanosheets further attached randomly and assembled into spheres superstructure. A schematic illustration of self-assembled $SrMoO_4$ sphere superstructures is shown in Scheme 1.

The Luminescence Characterization. The optical properties of as-prepared product were also studied. The infrared spectra of $SrMoO_4$ with different morphologies are shown in Figure 7. As we know, $SrMoO_4$ belongs to the scheelite family of structures with space group $I4_1/a$. The MoO_4^{2-} ion has tetrahedral symmetry, and it is represented as $\Gamma_{Td} = A_1(\nu_1) + E(\nu_2) + F_2(\nu_3) + F_2(\nu_4)$. Herein $A_1(\nu_1)$ and $E(\nu_2)$ are Raman active, but $F_2(\nu_3)$ and $F_2(\nu_4)$ are infrared active. The $F_2(\nu_3)$ vibrations are antisymmetric stretches, whereas the $F_2(\nu_4)$ vibrations are bending modes. The bands about 800 cm^{-1} are assigned to $F_2(\nu_3)$ antisymmetric stretching vibrations of $SrMoO_4$.[26,29] In our study, all samples exhibit the same peak at about 810 cm^{-1} corresponding to the vibration modes $F_2(\nu_3)$, which are consistent with those $SrMoO_4$ reported previously. This peak could be originated from the Mo−O stretching vibration of the MoO_4 group.[26,29] In previous reports, $SrMoO_4$ thin film possesses a weak absorption peak at 800 cm^{-1} because of its relatively larger size and lower crystallinity.[29]

Figure 8 shows the room-temperature photoluminescence spectra of the different morphologies using the same excitation wavelength of 237 nm. The spectra show that all of the three

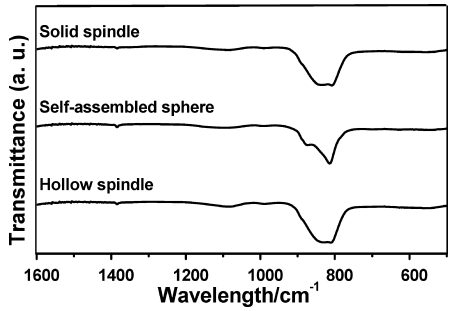

Figure 7. Infrared spectra of the obtained $SrMoO_4$ with different morphologies.

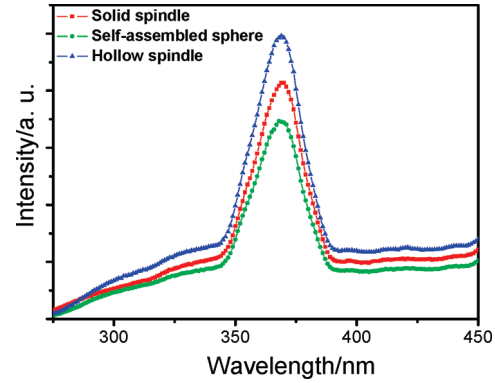

Figure 8. Room-temperature photoluminescence spectra of the obtained $SrMoO_4$ with different morphologies.

samples exhibited emission peaks at 369 nm. The emission peak might be ascribed to the charge-transfer transitions within the MoO_4^{2-} complex.[31,32,42−44] Ma et al. have synthesized $SrMoO_4$ with a microspindle structure through a microemulsion route, and they also possess similar PL emission at about 400 nm.[25] The other authors have observed the maximum emission of the PL emission at about 500 nm.[28−32,45,46] Compared with previous results, all $SrMoO_4$ samples synthesized by sonochemical method have an obvious blue-shifted PL emission because of their relatively small sizes and unique structures. The differences of maximum emissions wavelength can be assigned to the structural organization levels, preparation methods, treatment conditions, and different excitation wavelengths.[28] It is well-known that the relative intensity of the peaks varied, which indicates that they seem to be closely related to the morphology, size, surface defect states, and so on. The different shape and size would change the carriers excited from the valence band to the conduction band, and then finally result in the variations of luminescence.[47] In our case, it is interesting that the PL intensity of the hollow spindle sample is higher than that of the self-assembled sphere and solid spindle sample. The enhanced luminescence performance due to hollow spindle shape has large internal surface area at their interior and more surface defect than the other two samples.[48] Meanwhile, the self-assembled sphere sample possesses more surface defects, so they show more intensity PL emission than solid spindle sample. These results indicate that the luminescence properties of $SrMoO_4$ are very sensitive to its morphology and strongly dependent on structural defects.

Conclusion

In summary, self-assembled $SrMoO_4$ sphere superstructures composed of nanosheets have been successfully synthesized without any surfactants, template, and structure-directing reagents under ultrasonic treatment. Our experiment results indicated that by simply controlling pH value and addition of surfactant, different morphologies could be obtained. The formation mechanism of self-assembled $SrMoO_4$ sphere superstructure has been investigated. Different morphologies of $SrMoO_4$ show a similar PL emission peak at 369 nm under the 237 nm UV excitation, which is mainly attributed to the charge-transfer transitions. Furthermore, this method is highly possible to rapidly extend it as a general synthetic method for other metal molybdates.

Acknowledgment. This work is supported by the National Natural Science Foundation of China (Grant Nos. 20635020, 20821063, 20905001), the Project of Environmental Protection Department from Jiangsu Province (2008003), China Postdoctoral Science Foundation Funded Project (20080441027), and Jiangsu Planned Projects for Postdoctoral Research Funds (0802008B).

References and Notes

(1) Alivisatos, A. P. *Science* **1996**, *271*, 933.
(2) Hu, J. T.; Odom, T. W.; Lieber, C. M. *Acc. Chem. Res.* **1999**, *32*, 435.
(3) Mao, C. J.; Zhao, Y. X.; Qiu, X. F.; Zhu, J. J.; Burda, C. *Phys. Chem. Chem. Phys.* **2008**, *10*, 5633.
(4) Sun, Y.; Xia, Y. N. *Science* **2002**, *298*, 2176.
(5) Gou, L.; Murphy, C. J. *Nano Lett.* **2003**, *3*, 231.
(6) Yan, H. Q.; He, R. R.; Johnson, J.; Law, M.; Saykally, R. J.; Yang, P. D. *J. Am. Chem. Soc.* **2003**, *125*, 4728.
(7) Wu, C. Y.; Yu, S. H.; Antonietti, M. *Chem. Mater.* **2006**, *18*, 3599.
(8) Hu, Y. X.; Ge, J. P.; Yin, Y. D. *Chem. Commun.* **2009**, *8*, 914.
(9) Mdleleni, M. M.; Hyeon, T.; Suslick, K. S. *J. Am. Chem. Soc.* **1998**, *120*, 6189.
(10) Qiu, X. F.; Burda, C.; Fu, R. L.; Pu, L.; Chen, H. Y.; Zhu, J. J. *J. Am. Chem. Soc.* **2004**, *126*, 16276.
(11) Suslick, K. S. *Science* **1990**, *247*, 1439.
(12) Radziuk, D.; Shchukin, D.; Mohwald, H. *J Phys. Chem. C* **2008**, *112*, 2462.
(13) Mao, C. J.; Pan, H. C.; Wu, X. C.; Zhu, J. J.; Chen, H. Y. *J Phys. Chem. B* **2006**, *110*, 14709.
(14) Yi, G. S.; Sun, B. Q.; Yang, F. Z.; Chen, D. P.; Zhou, Y. X.; Cheng, J. *Chem. Mater.* **2002**, *14*, 2910.
(15) Yang, P.; Yao, G. Q.; Lin, J. H. *Chem. Commun.* **2004**, *7*, 389.
(16) Ryu, J. H.; Yoon, J. W.; Lim, C. S.; Oh, W. C.; Shim, K. B. *J. Alloys Compd.* **2005**, *390*, 245.
(17) Ivleva, L. I.; Basiev, T. T.; Voronina, I. S.; Zverev, P. G.; Osiko, V. V.; Polozkov, N. M. *Opt. Mater.* **2003**, *23*, 439.
(18) Yoshimura, M.; Ohmura, M.; Cho, W. S.; Yashima, M.; Kakihana, M. *J. Am. Ceram. Soc.* **1997**, *80*, 2464.
(19) Marques, A. P. D.; Melo, D. M. A.; Paskocimas, C. A.; Pizani, P. S.; Joya, M. R.; Leite, E. R.; Longo, E. *J. Solid State Chem.* **2006**, *179*, 671.
(20) Marques, A. P. D.; Melo, D. M. A.; Longo, E.; Paskocimas, C. A.; Pizani, P. S.; Leite, E. R. *J. Solid State Chem.* **2005**, *178*, 2346.
(21) Marques, A. P. A.; Dockal, E. R.; Skrobot, F. C.; Rosa, I. L. V. *Inorg. Chem. Commun.* **2007**, *10*, 255.
(22) Hitoki, G.; Takata, T.; Ikeda, S.; Hara, M.; Kondo, J. N.; Kakihana, M.; Domen, K. *Catal. Today* **2000**, *63*, 175.
(23) Hasan, M. A.; Zaki, M. I.; Kumari, K.; Pasupulety, L. *Thermochim. Acta* **1998**, *320*, 23.
(24) Spassky, D. A.; Ivanov, S. N.; Kolobanov, V. N.; Mikhailin, V. V.; Zemskov, V. N.; Zadneprovski, B. I.; Potkin, L. I. *Radiat. Meas.* **2004**, *38*, 607.
(25) Liu, J.; Ma, J. F.; Lin, B. T.; Ren, Y.; Jiang, X. H.; Tao, J. T.; Zhu, X. Y. *Ceram. Int.* **2008**, *34*, 1557.
(26) Lei, H. C.; Zhua, X. B.; Sun, Y. P.; Song, W. H. *J. Cryst. Growth* **2008**, *310*, 789.
(27) Thongtem, T.; Phuruangrat, A.; Thongtem, S. *Mater. Lett.* **2008**, *62*, 454.
(28) Sczancoski, J. C.; Cavalcante, L. S.; Joya, M. R.; Varela, J. A.; Pizani, P. S.; Longo, E. *Chem. Eng. J.* **2008**, *140*, 632.
(29) Marques, A. P. A.; Leite, E. R.; Varela, J. A.; Longo, E. *Nanoscale Res. Lett.* **2008**, *3*, 152.
(30) Liu, J. P.; Huang, X. T.; Li, Y. Y.; Li, Z. K. *J. Mater. Chem.* **2007**, *17*, 2754.
(31) Gong, Q.; Qian, X. F.; Ma, X. D.; Zhu, Z. K. *Cryst. Growth Des.* **2006**, *6*, 1821.
(32) Chen, D.; Tang, K. B.; Li, F. Q.; Zheng, H. G. *Cryst. Growth Des.* **2006**, *6*, 247.
(33) Zhang, Y. M.; Yang, F. D.; Yang, J.; Tang, Y.; Yuan, P. *Solid State Chem.* **2005**, *133*, 759.
(34) Zhou, Y. X.; Yao, H. B.; Zhang, Q.; Gong, J. Y.; Liu, S. J.; Yu, S. H. *Inorg. Chem.* **2009**, *48*, 1082.
(35) Luo, Z. J.; Li, H. M.; Shu, H. M.; Wang, K.; Xia, J. X.; Yan, Y. S. *Cryst. Growth Des.* **2008**, *8*, 2275.
(36) Lin, K. L.; Chang, J.; Zhu, Y. J.; Wu, W.; Cheng, G. F.; Zeng, Y.; Ruan, M. L. *Cryst. Growth Des.* **2009**, *9*, 177.
(37) Hu, T. J.; Gao, J.; Auweter, H.; Iden, R.; Lueddecke, E.; Wu, C. *Polymer* **2002**, *43*, 5545.
(38) Hayes, D.; Meisel, D.; Micic, O. I. *Colloids Surf.* **1991**, *55*, 121.
(39) Geng, J.; Zhu, J. J.; Lu, D. J.; Chen, H. Y. *Inorg. Chem.* **2006**, *45*, 8403.
(40) Ma, Y. R.; Qi, L. M.; Ma, J. M.; Cheng, H. M.; Shen, W. *Langmuir* **2003**, *19*, 9079.
(41) Hu, J. S.; Guo, Y. G.; Liang, H. P.; Wan, L. J.; Bai, C. L.; Wang, Y. C. *J. Phys. Chem. B* **2004**, *108*, 9734.
(42) Groenink, J. A.; Hakfoort, C.; Blasse, G. *Phys. Status Solidi A* **1979**, *54*, 329.
(43) Dinesh, R.; Fujiwara, T.; Watanabe, T.; Byrappa, K.; Yoshimura, M. *J. Mater. Sci.* **2005**, *41*, 1541.
(44) Ahmad, G.; Dickerson, M. B.; Church, B. C.; Cai, Y.; Jones, S. E.; Naik, R. R.; King, J. S.; Summers, C. J.; Kroger, N.; Sandhage, K. H. *Adv. Mater.* **2006**, *18*, 1759.
(45) Chen, L.; Gao, Y. *Chem. Eng. J.* **2007**, *131*, 181.
(46) Bi, J.; Cui, C. H.; Lai, X.; Shi, F.; Gao, D. J. *Mater. Res. Bull.* **2008**, *43*, 743.
(47) Wang, W. S.; Zhen, L.; Xu, C. Y.; Shao, W. Z. *Cryst. Growth Des.* **2009**, *9*, 1558.
(48) Gou, L. F.; Murphy, C. J. *Nano Lett.* **2003**, *3*, 231.

JP907525P